Implementation of a novel basement membrane invasion assay using mesenteric tissue

Ritobrata Ghose

CID: 00869298

Supervisor: Dr. Armando del Rio Hernandez

Co-Supervisor: Ernesto Cortes

Cellular and Molecular Biomechanics Laboratory, Department of Bioengineering

Imperial College London

This research report is submitted to fulfil the partial requirement of the degree of

MRes Cancer Biology

Department of Surgery and Cancer

Imperial College London

April 2018

Implementation of a novel basement membrane invasion assay using mesenteric tissue

Ritobrata Ghose[1,2], Ernesto Cortes[2,†], Alistair Rice[2,†], Dariusz Lachowski[2], Upamanyu Ghose[3], and Armando del Rio Hernandez[2,*]

1 Department of Surgery and Cancer, Imperial College London, UK.
2 Cellular and Molecular Biomechanics Laboratory, Department of Bioengineering, Imperial College London, UK.
3 Department of Computer Science, Manipal Institute of Technology, India.
† These authors contributed equally to the work

ABSTRACT

Metastasis accounts for nearly 90% of all cancer associated mortalities. A hallmark of metastasis, and more prominently in malignancies of epithelial origin such as in the pancreas, breast and liver, is invasion of the basement membrane (BM). Aggressive malignant tumour cells, empowered by the epithelial-to-mesenchymal transition program, lose their E-cadherin mediated cell-cell adhesion and adopt a mesenchymal phenotype leading to invasion of the BM. While various *in vitro* assays have been developed to address questions regarding the invasiveness of tumours with relation to the BM, most fail to recapitulate a physiologically accurate cell-membrane interface. One of the most commonly used models is a reconstituted gel matrix made from BM extract of the Engelbreth-Holm-Swarm tumour in mice. Commonly known as Matrigel, this 3D gel matrix has been widely used across a multitude of *in vitro* assays. However, apart from being expensive, it has been shown to influence cell behaviour. Here we introduce a novel 3D *in vitro* assay that uses the mouse mesenteric tissue as a mimic for the epithelial BM. We describe a simple, cost-effective protocol for extraction and setup of the assay, and show that the mesentery is a physiologically accurate model of the BM in its key components – type IV collagen, laminin-1 and perlecan. Furthermore, we introduce a novel quantification pipeline, Q-Pi, which allows the 3D reconstruction, visualisation and quantification of invasion at a cellular level. Overall, we demonstrate that the mesentery-based invasion assay provides a physiologically accurate tool to investigate BM invasion.

INTRODUCTION

The need for novel strategies to investigate the invasive capacity of tumours and in general, the underlying processes of metastasis, is arguably one of the primary requirements in the advancement of cancer diagnosis, prognosis and treatment. With the transition from non-lethal neoplasms to aggressive and invasive carcinomas being the principal cause for nearly 90% of all cancer associated mortalities (*1*, *2*), it is imperative to develop preventative strategies to deter tumour proliferation and dissemination (*3*). Metastasis is a complex multistep cascade (*4*, *5*) that can largely be divided into four distinct processes – (i) Loss of cell-cell/cell-extracellular matrix (ECM) adhesion and epithelial-to-mesenchymal transition (EMT), (ii) intravasation and survival in circulatory vessels, (iii) extravasation and mesenchymal-to-epithelial transition, and (iv) colonisation and proliferation in competent secondary organs. One approach towards breaking down these layers of complexity, is to focus individual studies on different aspects of the process.

A critical step following EMT in all cancers is the invasion of the basement membrane (BM). This process occurs more prominently in cancers of epithelial origin such as breast, lung and pancreas (*2*). Following the alterations of certain essential pro-oncogenic pathway components (*6*), proliferation cues such as loss of E-cadherin mediated adhesion (*7*) and nutrient deficiency based pro-invasion signalling (*8*) activate the development of invasion structures called invadopodia (*9*). These structures, orchestrated by the canonical Ras-like small GTPases – RhoA, Rac1 and Cdc42, promote BM transmigration (*10*). Successful invasion of the BM results in conversion of the underlying stroma into a reactive state which in turn induces an EMT positive feedback loop through various factors such as growth factor signalling (*11*) and stromal fibroblast (*12*, *13*) induced invasion.

The histologically distinct BM plays a critical role as a physical barrier between epithelial cells and the underlying stroma, and therefore prevents aggressive tumours from migrating into the stroma. The BM is a specialised ECM layer composed primarily of type IV collagen, laminins, perlecan and nidogen, and is basolateral to all epithelial and endothelial tissues in the body (Figure 1A; *14*). While type IV collagen and laminin individually assemble into superstructures, perlecan and nidogen function as linkers between the two, providing structural integrity (*14*, *15*). Moreover, perlecan, a heparin sulphate proteoglycan with multiple binding domains, also enables cell-ECM adhesion between collagen and laminin in the BM, and α-dystroglycans and sulfatide receptors on the cell surface (*16*).

To dissect the mechanisms surrounding the interaction between invasive carcinomas and the epithelial BM, a series of three-dimensional (3D) *in vitro* invasion assays have been explored in cancer research (Figure 1B-H; *17*). A common approach to represent the BM in *in vitro* invasion assays is the use of 3D gel matrices as a barrier, which provides a high-fidelity model to study cell migration and tissue remodelling in an appropriate signalling rich 3D microenvironment. While the most commonly used gel matrix is a BM extract from the Engelbreth-Holm-Swarm tumour (commercially Matrigel), type I collagen and other synthetic hydrogels are also used (*18*, *19*). Since these gels are reconstituted BM components, they are able to reproduce cell-cell, cell-ECM interactions and surface

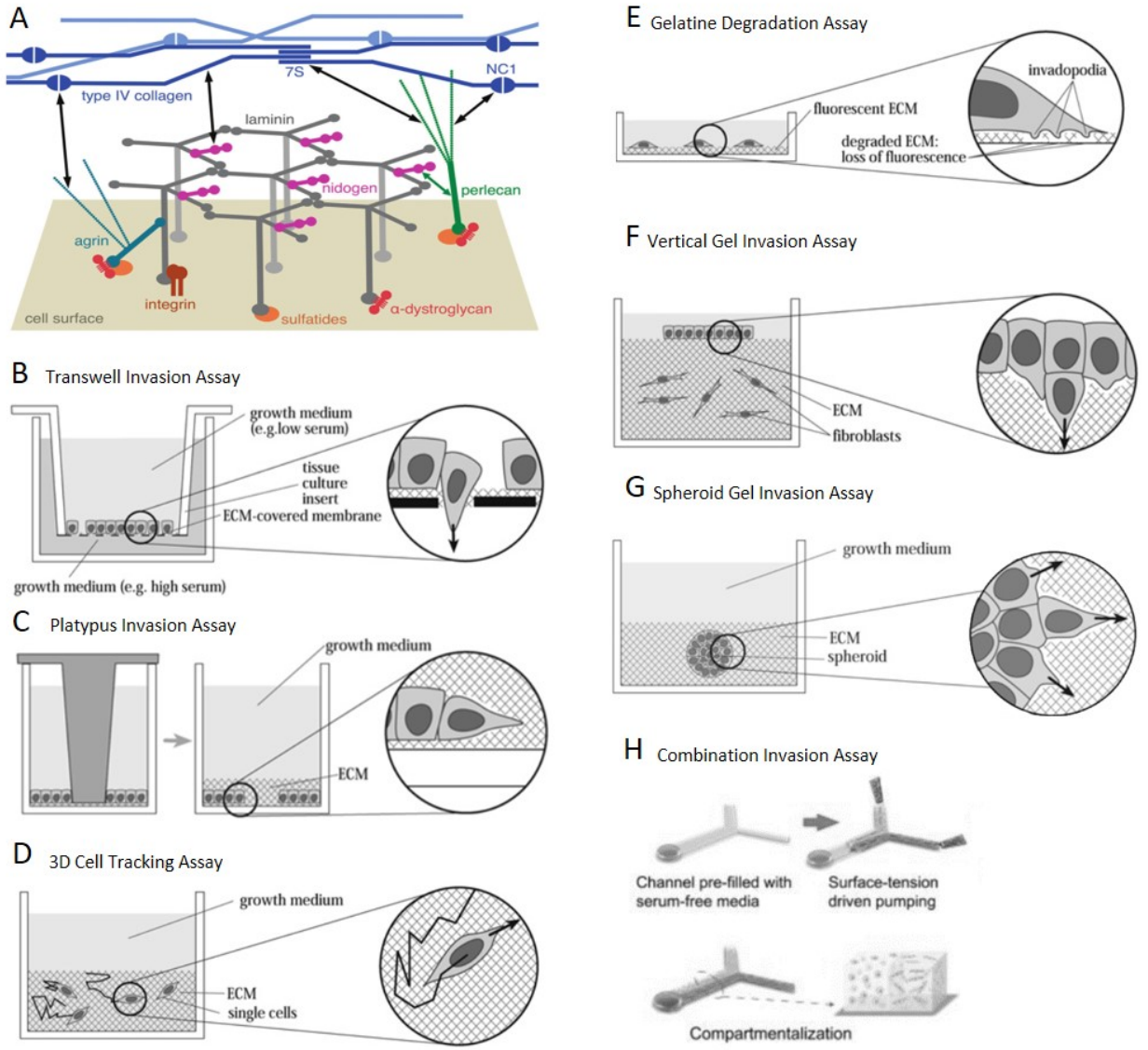

Figure 1. BM and BM invasion assays (A) The heterotrimeric laminin superstructure/network adheres to the cell surface through receptors (integrins, a-dystroglycan and sulfatides). A second superstructure/network is formed by type IV collagen. Perlecan, nidogen and agrin link collagen and laminin through interactions with its N-terminal 7S and C-terminal NC1 domain (black double-headed arrows). (B-H) A schematic representation of the various 3D in vitro invasion assays and (inset) showing their respective cell-ECM interfaces. (B) Transwell migration assay based on the Boyden chamber. A thin layer of reconstituted BM extract (BME) seeded over the permeable transwell membrane is used to represent the BM. (C) Platypus invasion assay. Cells are seeded using a stopper to spatially separate them. A BME gel is seeded on top of the cells and filling the gap. Invasion into the gel is studied. (D) 3D cell tracking assay. Cells are seeded onto a BME gel and their route tracked as they invade and migrate within the gel using automated microscopy and imaging systems. (E) Gelatine degradation assay. Cells are seeded onto layer of fluorescently labelled gelatine. Any loss of fluorescence is measured and quantified as a proxy for invasion structures (invadopodia). (F) Vertical gel invasion assay. Cells are seeded atop a BME matrix. The matrix may contain stromal fibroblasts and hence investigate the influence of other cell types on invasion. (G) Spheroid invasion assay. A 3D cell sphere is placed into a BME gel and studied for outward invasion of cells into the gel. (H) 3D spheroids and microfluidics based EMT assay. Laminar flow allows for two distinct compartments of polymer solutions containing 3D cell spheres. Figure in (A) was adapted from (*15*); (B-G) was adapted from (*17*), and; (H) was adapted from (*29*).

adhesion kinetics (*17*, *20*). A commonly used *in vitro* approach is the Transwell chemoinvasion assay which employs a version of the Boyden chamber to quantify invasion through a thin Matrigel layer towards a chemoattractant (Figure 1B; *21*, *22*). An epithelial compartment containing low serum media is seeded with cells, which are then allowed to cross the Matrigel layer and migrate into a high serum media which represents the stromal compartment.

Alternative assays have also been used to investigate aspects of tumour invasion by differently using these reconstituted matrices. The Platypus invasion assay uses two spatially separated cell populations seeded within a matrix to study the invasiveness of the cells (Figure 1C; *23*). Using a similar approach, the 3D Cell Tracking Assay, tracks the migration route of cells and studies various properties such as protease activity (Figure 1D; *24*). The gelatine degradation assay uses cells seeded atop a fluorescently labelled gelatine matrix to study invasion structures by quantifying degradation of the matrix as a proxy for invadopodia (Figure 1E; *25*). Although commercial availability and simple setups make these assays attractive and frequently used approaches in cancer research, one of their major caveats is the inability to maintain reproducible multicellular organisation in 3D (*19*).

To achieve a more reproducible and accurate representation of the dynamic processes in which other cell types facilitate invasion, more complex assays have been

developed. The vertical gel invasion assay uses a similar setup to that of the gelatine degradation assay with the addition of fibroblasts or other cell types seeded within a matrix to study their influence on invasion (Figure 1F; *12*). However, a more commonly used approach is the spheroid 3D cell co-culture system, which is an *in vitro* setup that allows the growth of one or more cell types in a 3D interaction environment (*26*). When used in conjunction with 3D gel matrices, these multicellular aggregates have served as important *in vitro* models in clinical and pre-clinical research of solid tumours due to their ability to closely replicate natural physiological factors (*20*, *26*, *27*). The spheroid invasion assay studies the outward migration of cells from a spheroid seeded within a gel matrix (Figure 1G). The possibility of consistently testing cell-cell interaction in 3D allows for the recapitulation of various naturally occurring interactions. However, while the spheroid assay has revealed and emphasized pivotal developmental clues in dynamic processes such as tumour complexity and heterotypic crosstalk (*28*), they are limited by factors such as size control and the inability to provide a holistic *in vivo* snapshot of processes such as host immune responses, metabolic waste disposal and limited nutrient supply (*20*).

To compensate for some of these shortfalls, combination systems that exploit 3D cell co-culture in association with microfluidics have been developed. For example, Sung *et al* reported a novel combination approach to investigate the transition of non-lethal ductal carcinomas in situ to invasive ductal carcinomas in breast cancer (Figure 1H; *29*). This method has established the importance of both cell-cell/cell-ECM contact and soluble factors, while providing insight into collagen organisation. Similarly, other approaches have led to the development of metastatic microenvironment (*30*) and tumour-endothelium interface models (*31*). The use of such combination strategies allows for a more intricate understanding of cellular kinetics and diffusion effects with higher spatio-temporal resolution. Other less frequently used experimental approaches such as cell printing and scaffold based fabrication of 3D matrices using novel biomaterials have also been described by Wang *et al* (*20*), Kramer *et al* (*17*). and Asghar *et al* (*27*).

A common challenge faced by all the current *in vitro* assays described above is an accurate depiction of the *in vivo* BM. While reconstituted gel matrices have had a fair share of success in addressing various questions surrounding BM invasion, their presence may inadvertently affect the invasion process. For example, Matrigel has been previously shown to enhance tumorigenicity and drug resistance in small cell lung cancer when injected into athymic mice (*32*). In contrast, another study shows no apparent influence on tumour development for neck and head cancer (*33*), implying the importance of context in the effects of Matrigel. Proteomics studies have discussed the presence of lowly abundant growth factors – tumour growth factor β, fibroblast growth factor, epidermal growth factor, platelet derived growth factor, insulin-like growth factor 1 and nerve growth factor – in Matrigel (*34*, *35*). Despite the availability of a growth factor reduced version of Matrigel (*36*), its potential in influencing cellular behaviour warrants caution in interpreting assay results. Taken together, these studies suggest that there is a need for a more physiologically accurate model to represent the epithelial BM.

Here we introduce the setup for a novel 3D *in vitro* assay that employs the mouse mesentery as a model for the epithelial BM. The mesenteric tissue is a lining of the peritoneum which orientates and attaches the intestine to the abdominal wall. Here, we describe a protocol for systematic retrieval of the tissue and confirm that the mesentery, as previously described (*13*, *37*), is indeed a suitable replica of the dense and complex BM structure. We also demonstrate the applicability of this assay in characterising the invasiveness of metastatic tumours at a cellular level. Furthermore, we introduce a novel quantification pipeline, Q-Pi, to quantitatively analyse invasion. Overall, our study presents an invasion assay that delivers a physiologically accurate BM model and offers a cost-effective tool to address impending questions in BM invasion.

MATERIALS AND METHODS

Mesentery extraction and decellularisation

Handling of animals was in strict accordance to the European and National Regulation for the Purposes. Extraction of mesentery was adapted from (*37*). Briefly, 9–12 months old wild type C57/B6 mice were euthanised, mesentery harbouring section of the intestine was retrieved and kept hydrated in Dulbecco's Phosphate Buffered Saline (PBS, Sigma Aldrich D8537). To extract the mesentery, cylindrical hollow scaffolds from cut 0.2 mL PCR tubes (VWR, USA, 732-0548) were fixed to the tissue using Vetbond tissue adhesive (3M, 1469sb) and then cut away from the intestine. Scaffolded mesenteries were then treated with 0.1% sodium azide (NaN_3, Sigma Aldrich S2002) in PBS for 30 min, decellularized in 1 M ammonium hydroxide (NH_4OH, Sigma Aldrich 09859) for 45 min and stored in PBS at 4°C for up to 1 week before use.

Cell culture and invasion assay

Pancreatic Ductal Adenocarcinoma (PDAC) cell line Suit2-007 (RRID:CVCL_B279) were cultured in complete media [high glucose Dulbecco's Modified Eagle's Media (Sigma Aldrich, D5671) supplemented with 10% heat-inactivated fetal bovine serum (Gibco 10500-064), 1% streptomycin/ penicillin cocktail (Sigma Aldrich, P4333), and 1% L-glutamine (Sigma Aldrich, G7513)] at 37°C and 5% CO_2.

For the invasion assay, scaffolded mesenteries were placed floating on complete media in 12-well plates. PDAC cells were resuspended in serum-free media, counted using a haemocytometer and 200,000 cells seeded per mesentery. The set up was allowed to incubate at 37°C and 5% CO_2. Mesenteries were transferred to new wells every 24 hours and fixed for imaging at 24, 120 and 240 hours using 4% paraformaldehyde (PFA, Sigma Aldrich P6148) in PBS, for 10–15 min.

Immunofluorescence

Staining of mesenteries and cells was adapted from (*37*). All steps were at room temperature. Briefly, fixed mesenteries were treated with permeabilisation buffer [0.5% Triton X-100 (Sigma Aldrich, T8787) in PBS] for 10 min and blocking buffer [1% bovine serum albumin (BSA, Sigma Aldrich,

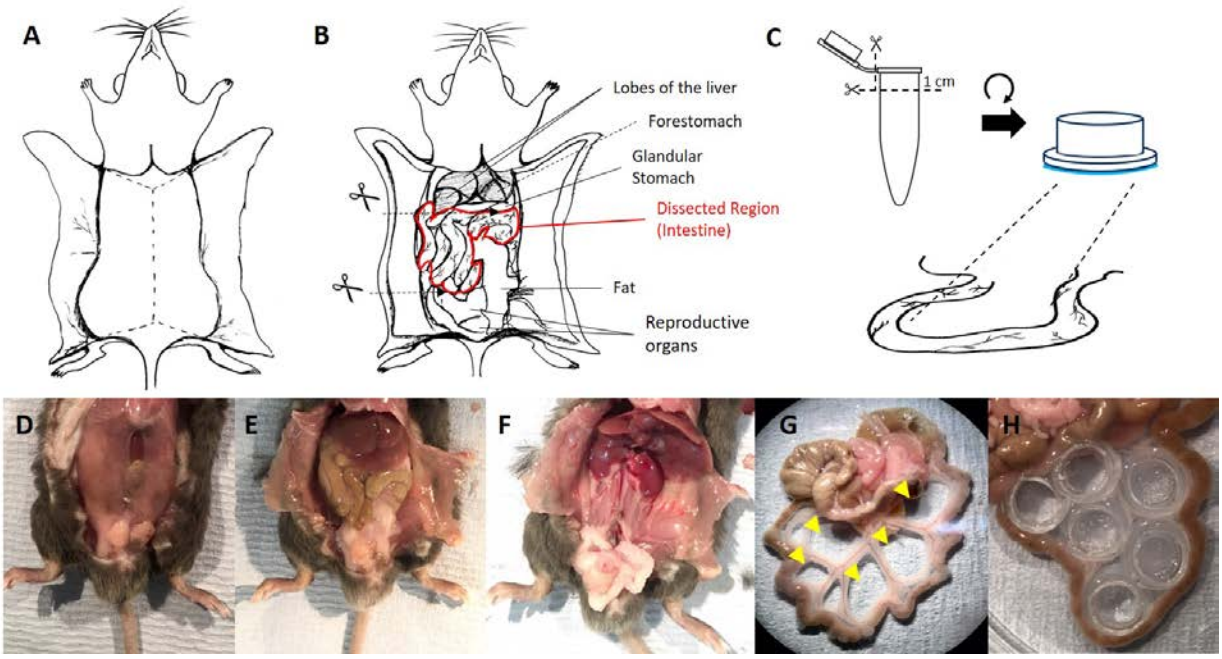

Figure 2. Extraction of the mesenteric tissue (A-C) A series of schematics representing the dissection and extraction of mesenteric tissue from mice as seen in the images in (D-H). (A) A vertical incision (dashed line) in the shape of an ' I ' from below the thorax to the pelvis reveals the peritoneal wall. (B) A second similar incision reveals the abdominal cavity. Incisions below the glandular stomach and above the rectum (scissors) release the intestinal region of interest (red border). (C) 0.2 mL PCR tubes are cut at 1 cm from the top, inverted and stuck onto mesentery using Vetbond tissue adhesive. (D) First incision showing peritoneum. (E) Second incision showing organs in the abdominal cavity. (F) Abdominal cavity after extraction. (G) Intestine with mesentery (yellow arrowheads) secured to the floor of a 90 mm petri dish using Vetbond. The tissue is kept hydrated in PBS. (H) Scaffolds are secured onto the mesentery using Vetbond.

A8022), 22.52 mg/mL Glycine (Sigma Aldrich, A8022) and 0.1% Tween 20 (Sigma Aldrich, P1379) in PBS] for 30 min. Primary antibodies [laminin-111 (Sigma Aldrich L9393), collagen IV (abcam ab19808) and perlecan (Santa Cruz Biotechnology sc-33707)] were diluted 1:100 in 1% BSA and 0.1% Tween 20 in PBS, and mesenteries treated for 60 min. Secondary antibodies [anti-Rabbit IgG (H+L) Alexa Fluor 488 (Thermo Fisher Scientific A-11008) and anti-Rabbit IgG (H+L) Texas Red (Thermo Fisher Scientific T-2767)] and Alexa Flour 546 Phalloidin (Thermo Fisher Scientific A22283) were diluted 1:200 in 1% BSA in PBS, and mesenteries treated for 60 min. All steps were separated by PBS washes.

Microscopy

Visualisation was done by obtaining ND2 confocal images of fluorescently tagged fixed samples using a NIKON Ti-Eclipse inverted microscope (NIKON, Japan) at 60X or 100X objective magnification and 0.2 µm z slices. Mounting was done by placing 25 µl of Prolong Gold Mountant with DAPI (Thermo Fisher Scientific P36931) on a rectangular glass cover slip, a mesentery was placed on it and another 25 µl of mountant above the mesentery. Samples were cured overnight at room temperature and imaged the following day.

Quantitative and statistical analysis

We developed a novel end-to-end Python2-based pipeline for 3D visualisation and Quantification of Percentage Invasion (Q-Pi). NIKON ND2 files were loaded using the *pims_nd2* library found at https://github.com/soft-matter/pims and then processed. The Q-Pi algorithm was coded in Linux and later optimised for the Windows operating system. The full library can be found at https://github.com/titoghose/Q-Pi. Graphing of processed invasion data and statistical analysis was done on GraphPad version 7.00 for Windows (GraphPad Software, La Jolla California USA). Kruskal-Wallis non-parametric test was used to compare average population invasions across days 1, 5 and 10. For significance $p<0.05$ = *; $p<0.01$ = **; $p<0.001$ = ***.

RESULTS

Retrieval and preparation of mesenteric tissue

The mouse mesentery is a particularly delicate tissue that requires dexterous and systematic retrieval in order to avoid damage and increase yield. We adapted a previously described protocol (*37*) and optimised it for mesentery extraction. Freshly sacrificed wild type mice were dissected to obtain mesenteries using hollow cylindrical scaffolds (Figure 2). We found that due to reduced stiffness and tissue coalescence, using mice sacrificed not more than 3 hours before dissection increased the number of mesenteries obtained per mouse from an average of 5 to 13. Although various dissection approaches were tested to optimise retrieval, we found the easiest access to be through a vertical incision in the shape of an ' I ' made on the ventral side from just below the thorax down to the pelvis (Figure 2 A, D). Keeping the peritoneal lining intact during the first incision ensured no damage to the intestine and hence the tissue. To gain access to the abdominal cavity, the peritoneal lining was cut using a second, more delicate ' I ' incision (Figure 2 B, E). To release the mesentery-harbouring-intestine from the rest of the gastrointestinal tract, two further incisions were made just below the glandular

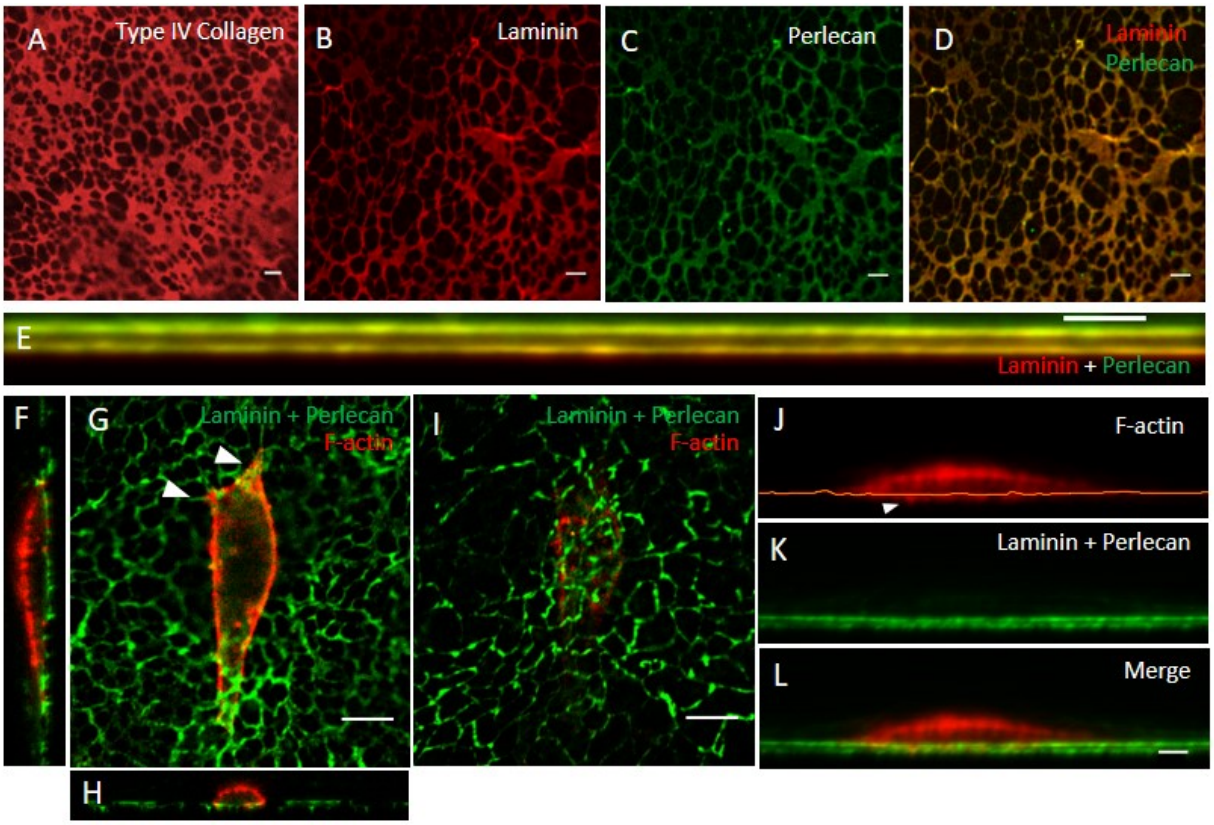

Figure 3. Visualisation of key mesentery components and cell-mesentery interactions. (A) Type IV collagen. (B) Laminin, (C) Perlecan, and (D) Laminin and perlecan merge showing co-localisation of the two proteins. (E) Laminin-perlecan bilayer (F-H) Seeded cell on laminin and perlecan bilayer. (G) Top view (XY plane) showing PDAC Suit2-007 cell present on top of the membrane with cell extensions (arrowheads). (F) Condensed z-tack view of cell in G, on the YZ plane. (H) Condensed z-tack view of cell in G, on the XZ plane. (I) Bottom view of the cell in G. (J) Visualisation of cell cytoskeleton from G showing invadopodia (arrowhead), (K) mesentery, and (L) cell invading mesentery. All scale bars are 5 µm.

stomach and above the rectum respectively (Figure 2 B). Although, the first incision can be made above the glandular stomach as well, we found that excluding the stomach from the extracted intestinal tract prevented contamination of subsequent steps due to leaked undigested contents. Next, to detach the region of interest from the abdomen, retroperitoneal attachments were incised. To do so, draping the intestines over one side of the abdominal cavity, rather than being held up using forceps, allowed easier access to the retroperitoneum without subjecting the mesentery to tear. The extracted intestine was kept hydrated in PBS.

Finally, to isolate the mesenteric tissue from the intestine, we designed and 3D printed hollow cylindrical scaffolds (Supplementary Figure 1). However, due to the prints being time consuming and failing to meet the miniscule and fragile requirements of the tissue, we adopted an alternate approach using 0.2 mL PCR tubes cut at about 1 cm height (Figure 2C). The cut 0.2 mL tube heads were fitted on to stretched-out mesenteries (Figure 2C, G, H) and the tissue was detached from the intestine using a scalpel to cut around the scaffold. Due to the highly elastic nature of the tissue, we found that it was easier to secure the intestine to the petri dish floor as in Figure 2G, before fitting the scaffolds. Alternatively, we also explored the possibility of incising some of the intra-mesenteric veins with the hope of relaxing the tissue, however this led to a decrease in the average number of mesenteries obtained.

To prepare the scaffolded mesenteries for the invasion assay, they were first treated with a solution of 0.1% sodium azide in PBS. Although we did not assess the criticality of this step, sodium azide treatment has been shown to improve fixation (*38*). The mesenteries were then washed in PBS and transferred to a 1 M ammonium hydroxide solution. Since the mesenteric tissue itself is acellular, the brief ammonium hydroxide treatment removes any adhering mesothelial cells.

Type IV collagen, laminin-1 and perlecan in the mesentery mimic the epithelial basement membrane

The mesenteric tissue has been shown to mimic the BM in its key structural components – type IV collagen, laminin-1 and perlecan (*13*, *37*). To validate the integrity of our extracted mesenteric tissue, fixed mesenteries were stained for type IV collagen, laminin-1 and perlecan as described previously (*37*) and imaged using confocal microscopy. However, our initial attempts yielded sub optimal images with non-specific and low intensity fluorescence (Supplementary Figure 2A). As a result, we introduced two new steps with the aim of improving the quality of staining. First, we found that increasing the duration of treatment with the permeabilisation buffer to 10 min, significantly improved intensity of fluorescence (Supplementary Figure 2B). Secondly, to address non-specific binding of antibodies, we introduced a blocking step prior to primary antibody addition, where mesenteries were treated to the blocking buffer for 30 min (Supplementary Figure 2C). Together, the new protocol delivered an optimised visualisation of the key structural components.

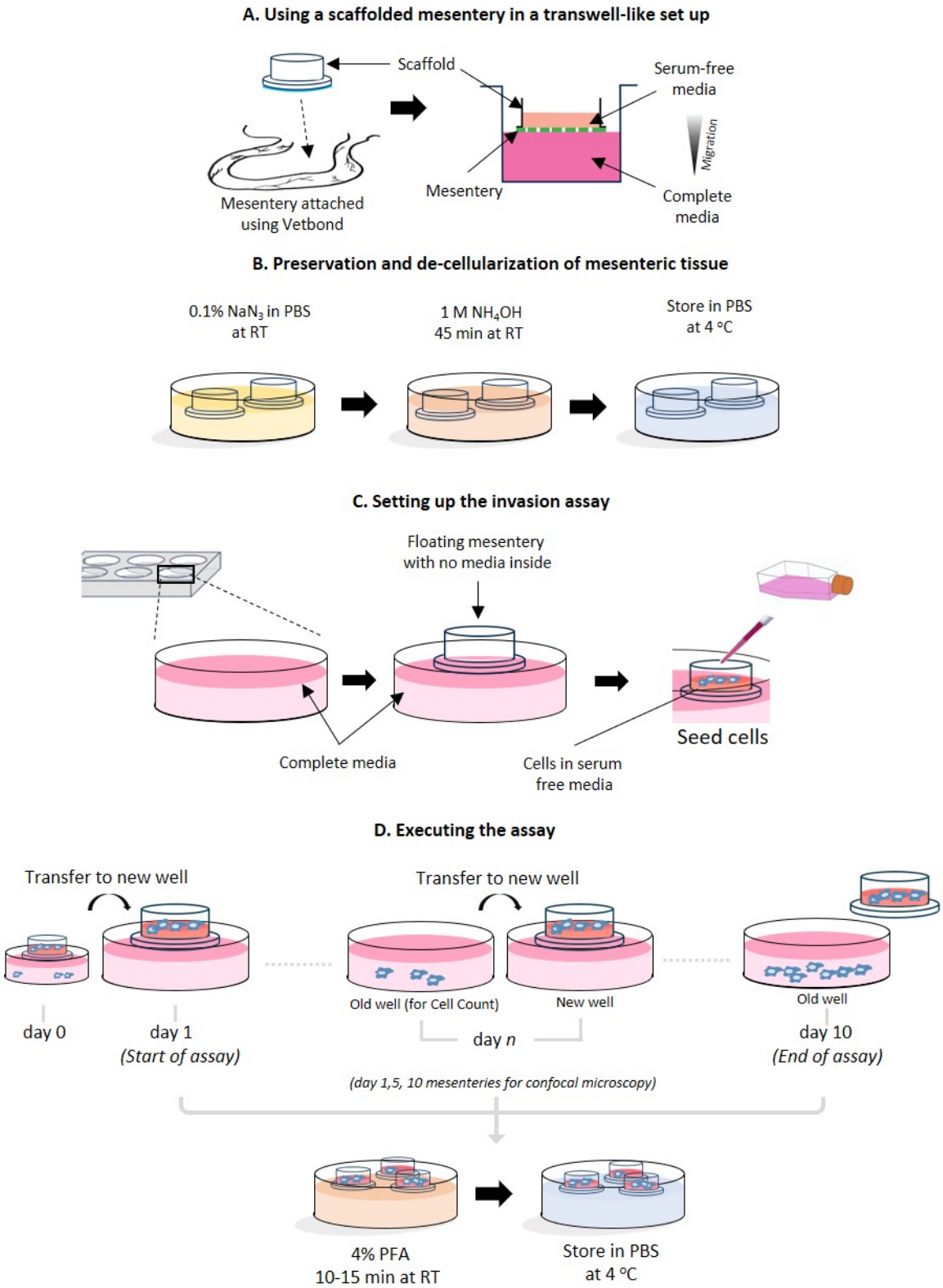

Figure 4. Setting up and execution of the invasion assay (A) Mesentery is extracted from the mouse as described earlier in Figure 2, and set up using a Transwell-like approach. The schematic (right) describes the chemical gradient (serum-free to complete media) used for the invasion assay. (B) Extracted mesenteries are processed in 50 mm petri dishes using 0.1% sodium azide (NaN_3) and 1 M ammonium hydroxide (NH_4OH) at room temperature (RT). Processed mesenteries can be stored in PBS at 4 °C for up to 1 week. (C) Set up of the invasion assay involves a 12-well plate where a well contains 2-3 mL complete media. Mesenteries are gently placed onto the media so as to allow them to float without seepage of media through the mesentery. Cell resuspension in serum-free media is seeded in the top compartment within the scaffold and cells allowed to migrate across the mesentery. (D) The assay is run from the 2nd day 'day 1' to the 11th day, 'day 10'. The first day is excluded to avoid biases introduced whilst seeding. Mesenteries are moved to a new well every 24 hours. The bottom of the 'old well' is then imaged for the cell count assay. For the mesentery invasion assay, days 1, 5 and 10 mesenteries are fixed in 4% PFA and stored in PBS.

We found that the key constituents of the BM – type IV collagen, laminin-1 and perlecan – were indeed well-established structures in the mesentery (Figure 3A-D). While type IV collagen had a perforated sheet-like appearance (Figure 3A), laminin and perlecan were more mesh-like in their structure (Figure 3B, C). Additionally, we also found that laminin and perlecan co-localised with each other and formed a distinctive bilayer (Figure 3D, E). Previous literature has shown that laminin polymerizes on cell surfaces directly through globular domains and indirectly by binding C-terminal heparin sulphate chains of perlecan (*15*, *16*). Perlecan in turn contains α-dystroglycan binding domains thereby creating a bridge between the heterotrimeric laminin and the α-dystroglycan receptors on the cell surface (*28*). Taken together, our findings indicate that the mesentery does indeed have BM-like characteristics where the bilayer represents a cell surface-binding perlecan sheet linked to a heterotrimeric laminin sheet.

A novel assay to study invasion of the epithelial BM

To set up the invasion assay, we adopted the Transwell invasion assay-like approach where scaffolded mesenteries were made to float on complete media in 12-well plates creating two distinct environments, one void of media (above the mesentery) and the other containing complete media (underneath the mesentery; Figure 4A, C). Here, the empty compartment serves as an epithelium from which cells invade the mesentery to move into the lower stromal compartment. PDAC cells were then collected by centrifugation and resuspended in the low nutrient serum-free media and seeded onto the mesentery. We found that given the area of our scaffolds, 200,000 cells per mesentery was ideal to prevent clustering and hence facilitate imaging at later stages. Additionally, we also found that seeding volumes of cell suspension greater than 10-15 µL per mesentery increased the likelihood of media cross contamination and cell spillage. To address this issue of a possible bias introduced whilst seeding, scaffolds were transferred to a new well after the first 24 hours, therein marking 'day 1' and the beginning of the invasion assay (Figure 4D).

The mesenteries were incubated at 37°C and 5% CO_2 and monitored every 24 hours for a period of 10 days. Our initial qualitative observations suggested an increase in invasion from day 1 to day 10 after which there was minimal invasion. Although theoretically imaging samples every 24 hours was ideal for analysis, we argued that to practically test the functionality of the invasion assay, data collection on days 1, 5 and 10 were sufficient. To that end, mesenteries containing invading cells were washed, fixed and stained at 24, 120 and 240 hours each (Figure 4D). Then, using confocal microscopy, we visualised the mesenteries (stained for the laminin-perlecan bilayer) and cells (stained for cytoskeleton using fluorescently labelled phalloidin) to test for successful adhesion and invasion (Figure 3F-L). We found that cells were able to attach and produce invadopodia (Figure 3G, J), hence indicating an active invasion processes. We were also able to easily distinguish between the bilayer and cell cytoskeleton using multi-channel fluorescence imaging, (Figure 3J-L). Together, we were able to visualise attachment of cells on the XY plane, as well as invasion of the mesentery on the YZ and XZ planes.

Q-Pi: A novel tool to quantify invasion

One of our primary objectives when designing the invasion assay was to be able to realistically present the tumour-membrane interface and reproduce an accurate quantitative report on the aggressiveness and invasiveness of metastatic tumours. While most *in vitro* assays employ an invasion cell count approach to address the quantification of invasion (*39*), they fail to report on the cell-membrane interactions and often include heavy human judgment on factors such as thresholding. We argued that an automated tool to visualise and quantify invasion with relation to the cell-membrane interface would provide greater resolution to the invasion data. To that end, we developed a novel Python based 3D reconstruction pipeline for the Quantification of Percentage Invasion, Q-Pi (Figure 5A), keeping in mind two specific aims. First, we wanted to reduce human bias and hence increase accuracy and efficiency of analysis. We argued that creating an automated quantification pipeline would limit human intervention to only image input and the high-throughput nature of the analysis would allow quantification of large populations thereby reducing error. Secondly, given our access to a more biologically relevant BM model, we wanted to quantify cell-membrane interactions at a higher resolution and hence focussed on the interface between a single cell and the membrane.

The algorithm is an end-to-end pipeline that directly imports confocal microscopy images of fixed mesenteries on days 1, 5 and 10 using the *pims_nd2* python library and passes them through a series of image processing blocks. Briefly, Q-Pi uses a bilateral filter to identify cell edges followed by a binary thresholding function to reduce unwanted noise (Figure 5B-C). Then it applies two morphological transformations, namely erosion and dilation, to correct for noise missed by the thresholding step or parts of the cell mistaken for noise (Figure 5D-E). Next, it employs the Teh-Chin89 chain approximation algorithm (*40*) to identify cell contours as a set of points in two-dimensional Euclidean space, which are then fitted using a best ellipse approximation (Figure 5F-G). And finally, the Convex Hull algorithm (*41*) allows for reconstruction of the cell in 3D using the elliptical coordinates (Figure 5H). Using this reconstructed cell, and a manually obtained z-stack corresponding to the BM, the percentage volume of cell under the top layer of the membrane is calculated.

While testing various options to increase the efficacy of the algorithm, we found that using a bilateral filter as opposed to other standard filters such as the Gaussian filter, offers a more optimal combination of edge preservation and noise reduction, as previously described (*42*). We also found that in cases where the raw images have minimal noise and the cell structure is consistent, avoiding the best ellipse approximation may provide more accurate reconstructions. In contrast, in cases where the raw images were high in noise due to bleed through from multi-channel microscopy, there remained the likelihood of overestimating invasiveness. To troubleshoot this and test its influence on quantification, we repeatedly ran the algorithm on the same populations using the same images. Although bleed through across channels caused a marginal overestimation of the cell volume and percentage invasion at the cellular level, the algorithm was deterministic without exception and hence

produced consistent results for the same input image. Moreover, since invasion assay analysis is typically comparative in nature, this did not affect the relative percentage invasion across populations between different days in the assay.

Quantifying invasion across the mesentery

To validate our invasion assay, we analysed the progression of aggressive PDAC Suit2-007 cells across the mesenteric tissue. On day 1 (24 hours post seeding), we observed cells that had invaded to a minimal degree, showing no noteworthy remodelling of the membrane (Figure 5I). In contrast, on day 5 (120 hours post seeding) we found cells embedded significantly deeper into the membrane with a certain degree of reconstruction (Figure 5J). In most cases we found breaks in the top layer followed by a depression in the lower layer of the membrane. This is most likely caused due to factors such as force-mediated breaching (*2*) and metalloproteinase induced degradation (*43*). However, in some rarer instances, degradation was visible in larger regions surrounding the invading cell, possibly representing a more advanced stage in the invasion process (not shown). Instances where cells were completely invaded, primarily in day 5 and 10 populations, the bilayer of the mesentery was apparent, and the top layer of the membrane appeared reconstructed over the cell (Figure 5K).

To further evaluate the potential of the assay, we used Q-Pi for a more comprehensive visualisation and quantification of percentage invasion. 3D reconstructions of invading cells showed a significant change in the status of invasion from day 1 to 10 (Figure 5L-N). Additionally, we used 3D reconstructions to quantify invasion at a cellular level across populations on day 1, 5 and 10 and found a significant increase between day 1 and 5 from 12% to 70%, but a decrease between day 5 and 10 from 70% to 30% (Figure 5O). We argued that a likely explanation for the counter intuitive decrease was a loss of data representing the cells falling through the lower layer of the membrane.

To address this issue, we used the classical invasion cell count assay as a secondary mode of quantification. In addition to the original set up of the invasion assay, as described above, mesenteries were transferred to new wells every 24 hours and the bottom of old wells imaged (Figure 4D). For each well/mesentery, several regions of interest (ROI) were imaged and quantified as average number of cells per ROI per mesentery. As expected, the cell count assay accounted for the lost data and revealed a continuous increase in invasion from day 1 to day 10 (Figure 5P). We found a linear increase in the number of average invaded cells per ROI per mesentery, from 11 on day 1 to 28 on day 10. Taken together, the Q-Pi and cell count data validate this novel mesentery-based chemoinvasion assay as a tool to study the invasiveness of metastatic tumours. A complete step-by-step approach for the invasion assay with cell count has been described in Supplementary Figure 3.

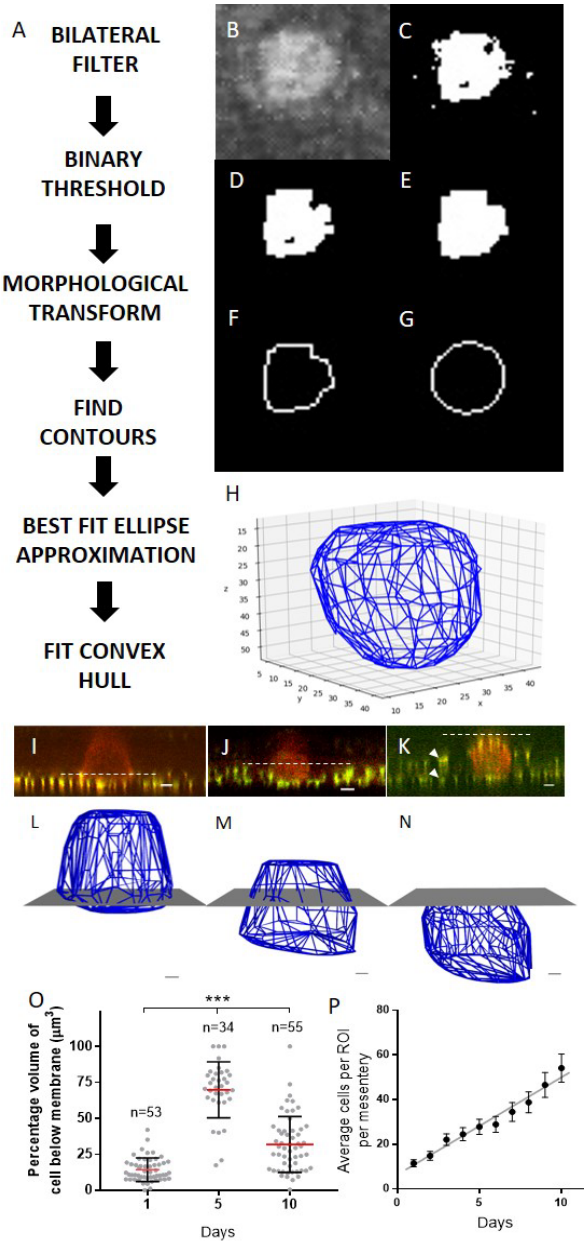

Figure 5. Quantification of Percentage Invasion (Q-Pi) algorithm (A) Q-Pi Quantification Pipeline: Sequence of processing blocks to arrive at cell reconstruction. (B) View of cell post application of bilateral filter. (C) Cell extracted from background after applying binary threshold function. (D, E) Refined cell boundaries after applying morphological transformations i.e. opening [erosion-dilation] and closing [dilation-erosion]. (F) Contour fit on the cell to get coordinates of each cell z-slice in two-dimensional Euclidean space. (G) Best fit ellipse approximation to compensate for segments of the cell that were ignored in thresholding due to irregular lighting. (H) 3D plot of the reconstructed cell after application of Convex Hull algorithm. (I-K) Representative images of invading cells on day 1, 5 and 10 respectively in relation to the top layer of the basement membrane (dashed white line). (I) Very minimal invasion is seen on day 1. (J) On day 5, the membrane is seen pressed down by the force exerted by the invading cell, placing approximately 65% of the cell below the top layer. (K) On day 10, the membrane can be seen covering the top of the cell which is 100% below the membrane top layer. The laminin-perlecan bilayer is clearly visible here (arrowheads). (L-N) Representative Q-Pi generated 3D cell reconstructions with respect to the membrane. (L) Day 1 cell shows approximately 12% cell volume under membrane. (M) Day 5 cell shows approximately 70% cell volume under membrane. (N) Day 10 cell shows 100% volume under membrane. (O) Q-Pi generated percentage cell invasion for populations on day 1, 5 and 10. n represents the number of cells quantified to produce population statistics in each ($p<0.0001$ = ***, Kruskal-Wallis non-parametric test). Black capped bars represent standard deviation, and red bar represents mean. (P) Invasion cell count assay results showing linear

DISCUSSION

Invasion of the BM represents a critical milestone in the onset of tumour metastasis and *in vitro* systems are required to address fundamental questions about regulation of the

(R^2 = 0.969) increase in cumulative invasion from day 1 to 10. Each point is the cumulative sum of the mean values for each day, with standard error for each day calculated as the sum of standard errors for all the days used in summation. Number of regions imaged per well was normalised depending on the number of mesenteries. For day 1 to 10, average number of regions imaged per well = 13, 21, 23, 13, 21, 10, 17, 12, 13, 16. Scale bars in (I-K) are 10 µm and (L-N) are 2 µm.

invasion process. Various assays have been previously developed, such as the Transwell invasion assay and spheroid cell culture assays, though many lack the ability to represent a physiologically accurate membrane (*17*, *20*, *27*). Here, we have combined the simplicity and rapidity of *in vitro* assays with the physiological accuracy of *in vivo* models to develop a novel *in vitro* invasion assay using the mouse mesentery as a model for the BM. Other *in vivo* models have been developed to accurately represent the BM, such as the anchor cell invasion model in *Caenorhabditis elegans*. However, while studies in *C. elegans* have shed light on regulators of the process such as nuclear hormone receptor-67 (*44*), an ortholog of a human tailless transcription factor, the distant homology of *C. elegans* to the human genome impedes the translation to therapeutics. Our use of a mouse mesentery is advantageous as it is extracted from a species closer to humans and has been verified as similar in composition to the *in vivo* BM in humans.

The use of the mouse mesentery as a BM mimic in invasion assays was previously explored by Schoumacher *et al* (*37*) and here we further develop this protocol. However, the mesentery as a model had been neglected until recently when Glentis *et al.* used it in an assay to show the ability of cancer-associated fibroblasts to induce metalloproteinase-independent invasion (*13*). Following these results, we decided to use the mesentery in developing a cost-effective and standardized protocol for an invasion assay. More specifically, the aims of our study were to optimise extraction of the mouse mesenteric tissue, validate its ability to mimic the BM composition, and to demonstrate the ability of the assay to characterise and quantify invasion. The chemoinvasion assay described in our study requires undamaged membranes to maintain a chemical gradient. Hence, the proper retrieval of the tissue is an important aspect of the assay. While we adapted the previous protocol for extraction of the mesentery, here we describe some critical observations that improve the systematic and careful retrieval of the tissue. Although various approaches can be used for extraction, given the delicate nature of the tissue, it was important to develop a systematic protocol to optimise the process and reduce loss of mesentery due to damage. Additionally, to overcome the high cost of commercially available Transwells, we demonstrated the use of cost-effective scaffolds that can be easily manufactured from PCR tubes and still replicate the functionality of the widely used Boyden chamber-inspired setup (*22*).

Another major component of this study was to confirm the structural similarity of mesenteries to BMs *in vivo*, as previously described (*13*, *37*). One defining feature of the epithelial BM is its fibrillar bilayer structure, studied in the retinal inner limiting membrane (*45*), and more recently by our lab in the pancreas BM (unpublished, Rice, *et al*). In this study, we were able to show that the mesentery is a composite structure made of type IV collagen, laminin-1 and perlecan which are the most abundant components of the epithelial BM (*14*). Additionally, we also found that it has a characteristic bilayer. Taken together, these findings attribute BM-like similarity to the mesentery and confirm its potential as a physiologically accurate model. In comparison, BM extract-based gel matrices such as Matrigel, are also composed of type IV collagen, laminin-1 and perlecan (*36*). However apart from being expensive (£86 /mL, Sigma Aldrich), they have batch-to-batch variation and contain a multitude of growth factors which may lead to biases in results (*35*). These aspects argue a preference for the mesentery over reconstituted gel matrices to recreate more physiologically accurate invasion assays.

A factor not widely explored in our study was the structural variation across different epithelial BMs (*14*). For example, one of the major reasons for BM structural diversity is a multitude of laminin isoforms (*15*). Although we use only laminin-1 here, which represents the most commonly occurring α1β1γ1 chain composition, 15 other isoforms (different combinations of α-, β-, γ- chains) have been detected across various BMs (*14*). Since recent work in our lab has established the abundance of laminin-1 in the pancreas BM, we decided to test our invasion assay using PDAC Suit2-007 cells. The aggressive and invasive nature of these pancreatic cancer cells make them an excellent candidate to test the functionality of the invasion assay (*46*). In the future however, by validating the presence of other isoforms or characteristic structural components from different BMs, the mesentery can be used to study invasion in a multitude of other cancers.

Future development of the assay could involve a multitude of modifications that answer additional questions surrounding the invasion process. For example, the assay can be used to test the repressive potential of novel migrastatic drugs as a therapeutic solution (*47*). Additionally, by modifying the set-up, the assay can be tailored to assess various invasion factors. In our study we use complete media as a chemoattractant to loosely represent an active stroma, however, more elaborate collagen-fibroblast mixtures have been used (*13*). By altering the composition of the stromal compartment, using ECM proteins or additional chemoattractants such as growth factors, future assays could allow a more detailed analysis of regulation of invasion. Another approach that could potentially further the outcome of the assay is the use of elastic pillars, a method of traction force microscopy. These pillars are arrays of finger-like 1 µm wide silicone structures that allow measurement of force. Previously they have been used to study changes in cell structure and differences between cell body and cell extensions (*48*). By placing these arrays just below the membrane and imaging force generation by invaded cells that land on them, one could potentially obtain high-resolution snapshots of changes in cytoskeletal force generation. Combining this technique with immunofluorescence staining for contractility markers such as phosphorylated myosin light chain could further enhance this analysis. Furthermore, live cell imaging through fluorescent labelling of the mesentery and cells may be possible for comprehensive analysis, though careful protocol development would be required to prevent interference in the invasion process. This assay therefore opens new avenues for exploration.

A further advantage of this assay is the ability to analyse the mesentery and cells after the invasion process and begin to

delineate the events that have occurred during invasion. Using immunofluorescence and systematic image acquisition, we were able to closely investigate cells and changes in their structure. We showed that the PDAC cells successfully attached to the mesenteries and produced invadopodia as an indication of active invasion. Moreover, using the fluorescently tagged mesenteric bilayer, we were able to capture the various stages of matrix remodelling and force-mediated breakages as cells invaded the membrane. Cell stiffness (*49*, *50*) and force-dependent breaching of the membrane (*2*) are important factors that have been recently shown to play a major role in EMT and chemoinvasion. While we have captured structural changes in cell cytoskeleton and the mesentery using immunofluorescence, further analysis using quantitative approaches such as atomic force microscopy can provide information on cell and matrix stiffness. By measuring the mechanical properties of samples, atomic force microscopy can offer a high-resolution understanding of cells and membranes, thus enhancing our understanding of the cell-membrane interface.

Finally, one of the major outlooks during the development of this assay was to establish a standardized quantification strategy that would allow for comprehensive visualisation and quantification of invasion. Previously, techniques such as manual counting and quantification of stained cells have been used to study invasiveness in gel-based assays at a population level (*39*, *51*). However, such approaches are prone to human influence. We developed Q-Pi as an automated alternative to reduce subjectivity in analysis and quantify invasion at a high resolution. In comparison to other available computer software as highlighted by Castillo *et al* (*52*), Q-Pi is beneficial as an open source program available to run across multiple platforms as a cost-effective and versatile algorithm. Its simplicity and high-throughput nature, limiting human involvement to just image acquisition and input, makes it an easy and quick setup tool. Nevertheless, the algorithm is in its initial stages and not fully robust to imperfections in image acquisition such as cross-channel bleed-throughs during confocal microscopy. As a result, we intend to further its development by addressing two key components – removal of ellipse approximations and improving of the thresholding function to attribute robustness against irregularities in image acquisition. Overall, we believe Q-Pi is able to successfully represent changes in invasion at a cellular level, and to our knowledge, is the only algorithm of its kind used to recreate and quantify invasion based on a cell-membrane interface in 3D. Few other computerised approaches have been tested (*52*, *53*), however they majorly focus on entire tumours as opposed to cellular-level quantification. Having demonstrated its functionality through the mesentery invasion assay in this study, as well as through other assays in our lab (unpublished, Rice *et al*), we believe that Q-Pi has the potential to become a standardized approach to investigate cell-membrane interactions.

In conclusion, this study describes the implementation of a novel invasion assay using the mouse mesentery as a physiologically accurate model for the BM. We have demonstrated the close structural resemblance between mesentery and BM and tested the validity of the invasion assay using PDAC cells. Furthermore, we developed and validated a novel algorithm, Q-Pi, which enables the 3D visualisation and high-throughput quantification of invasion at a cellular level. And finally, we discussed the limitations and future potential of this study.

Author contributions and acknowledgment

R.G. conducted experiments, together with E.C., A.R. and D.L.. E.C. and A.R. were instrumental in optimisation of adapted protocols. D.L. was involved in optimisation of immunofluorescence and imaging. Q-Pi was conceived by R.G. and developed together with U.G. The manuscript was written by R.G. and proofread and corrected by E.C., A.R., and A.d.R.H. Additionally, we thank the Ocular Biomechanics Laboratory, Imperial College London for providing the mice, and all the team members of the Cellular and Molecular Biomechanics Laboratory for their support and inputs.

References

1. P. Mehlen, A. Puisieux, Metastasis: A question of life or death. *Nat. Rev. Cancer*. **6**, 449–458 (2006).
2. T. T. Chang, D. Thakar, V. M. Weaver, Force-dependent breaching of the basement membrane. *Matrix Biol.* **57–58**, 178–189 (2017).
3. V. Mittal, Epithelial Mesenchymal Transition in Tumor Metastasis. *Annu. Rev. Pathol. Mech. Dis*. **13**, 395–412 (2018).
4. J. A. Joyce, J. W. Pollard, Microenvironmental regulation of metastasis. *Nat. Rev. Cancer*. **9** (2009), pp. 239–252.
5. F. Van Zijl, G. Krupitza, W. Mikulits, Initial steps of metastasis: Cell invasion and endothelial transmigration. *Mutat. Res. - Rev. Mutat. Res.* **728**, 23–34 (2011).
6. L. G. Pedraza-Fariña, Mechanisms of oncogenic cooperation in cancer initiation and metastasis. *Yale J. Biol. Med.* **79**, 95–103 (2006).
7. U. Cavallaro, G. Christofori, Cell adhesion and signalling by cadherins and Ig-CAMs in cancer. *Nat. Rev. Cancer*. **4**, 118–132 (2004).
8. D. H. Kim *et al.*, mTOR interacts with raptor to form a nutrient-sensitive complex that signals to the cell growth machinery. *Cell*. **110**, 163–175 (2002).
9. J. V. Small, T. Stradal, E. Vignal, K. Rottner, The lamellipodium: Where motility begins. *Trends Cell Biol.* **12**, 112–120 (2002).
10. C. D. Nobes, A. Hall, Rho, Rac, and Cdc42 GTPases regulate the assembly of multimolecular focal complexes associated with actin stress fibers, lamellipodia, and filopodia. *Cell*. **81**, 53–62 (1995).
11. F. Van Zijl *et al.*, Hepatic tumor-stroma crosstalk guides epithelial to mesenchymal transition at the tumor edge. *Oncogene*. **28**, 4022–4033 (2009).
12. C. Gaggioli *et al.*, Fibroblast-led collective invasion of carcinoma cells with differing roles for RhoGTPases in leading and following cells. *Nat. Cell Biol.* **9**, 1392–1400 (2007).
13. A. Glentis *et al.*, Cancer-associated fibroblasts induce metalloprotease-independent cancer cell invasion of the basement membrane. *Nat. Commun.* **8** (2017), doi:10.1038/s41467-017-00985-8.

14. V. S. LeBleu, B. Macdonald, R. Kalluri, Structure and function of basement membranes. *Exp. Biol. Med. (Maywood).* **232**, 1121–9 (2007).
15. E. Hohenester, P. D. Yurchenco, Laminins in basement membrane assembly. *Cell Adhes. Migr.* **7**, 56–63 (2013).
16. J. F. Talts, Z. Andac, W. Göhring, A. Brancaccio, R. Timpl, Binding of the G domains of laminin α1 and α2 chains and perlecan to heparin, sulfatides, α-dystroglycan and several extracellular matrix proteins. *EMBO J.* **18**, 863–870 (1999).
17. N. Kramer *et al.*, In vitro cell migration and invasion assays. *Mutat. Res. - Rev. Mutat. Res.* **752**, 10–24 (2013).
18. D. R. Stamov, T. Pompe, Structure and function of ECM-inspired composite collagen type I scaffolds. *Soft Matter*. **8**, 10200 (2012).
19. C. P. Huang *et al.*, Engineering microscale cellular niches for three-dimensional multicellular co-cultures. *Lab Chip*. **9**, 1740 (2009).
20. C. Wang *et al.*, Three-dimensional in vitro cancer models: A short review. *Biofabrication*. **6** (2014), , doi:10.1088/1758-5082/6/2/022001.
21. A. Albini *et al.*, A Rapid in Vitro Assay for Quantitating the Invasive Potential of Tumor Cells, 3239–3246 (1987).
22. A. Albini, R. Benelli, The chemoinvasion assay: A method to assess tumor and endothelial cell invasion and its modulation. *Nat. Protoc.* **2**, 504–511 (2007).
23. S. O. Lim, H. Kim, G. Jung, P53 inhibits tumor cell invasion via the degradation of snail protein in hepatocellular carcinoma. *FEBS Lett.* **584**, 2231–2236 (2010).
24. M. H. Zaman *et al.*, Migration of tumor cells in 3D matrices is governed by matrix stiffness along with cell-matrix adhesion and proteolysis. *Proc. Natl. Acad. Sci. U. S. A.* **103**, 10889–94 (2006).
25. J. Anderl, J. Ma, L. Armstrong, Fluorescent Gelatin Degradation Assays for Investigating Invadopodia Formation. *Nat Methods*. **121007**, 1–6 (2012).
26. L. A. Kunz-Schughart, J. P. Freyer, F. Hofstaedter, R. Ebner, The use of 3-D cultures for high-throughput screening: The multicellular spheroid model. *J. Biomol. Screen.* **9**, 273–285 (2004).
27. W. Asghar *et al.*, Engineering cancer microenvironments for in vitro 3-D tumor models. *Mater. Today*. **18**, 539–553 (2015).
28. M. R. Junttila, F. J. De Sauvage, Influence of tumour micro-environment heterogeneity on therapeutic response. *Nature*. **501**, 346–354 (2013).
29. K. E. Sung *et al.*, Transition to invasion in breast cancer: a microfluidic in vitro model enables examination of spatial and temporal effects. *Integr. Biol.* **3**, 439–450 (2011).
30. A. Y. Hsiao *et al.*, Microfluidic system for formation of PC-3 prostate cancer co-culture spheroids. *Biomaterials*. **30**, 3020–3027 (2009).
31. I. K. Zervantonakis *et al.*, Three-dimensional microfluidic model for tumor cell intravasation and endothelial barrier function. *Proc. Natl. Acad. Sci.* **109**, 13515–13520 (2012).
32. R. Fridman *et al.*, Reconstituted basement membrane (matrigel) and laminin can enhance the tumorigenicity and the drug resistance of small cell lung cancer cell lines. *Proc. Natl. Acad. Sci. U. S. A.* **87**, 6698–6702 (1990).
33. F. P. Fliedner, A. E. Hansen, J. T. Jørgensen, A. Kjær, The use of matrigel has no influence on tumor development or PET imaging in FaDu human head and neck cancer xenografts. *BMC Med. Imaging*. **16**, 1–8 (2016).
34. S. Vukicevic *et al.*, Identification of multiple active growth factors in basement membrane matrigel suggests caution in interpretation of cellular activity related to extracellular matrix components. *Exp. Cell Res.* **202**, 1–8 (1992).
35. G. Benton, I. Arnaoutova, J. George, H. K. Kleinman, J. Koblinski, Matrigel: From discovery and ECM mimicry to assays and models for cancer research. *Adv. Drug Deliv. Rev.* **79**, 3–18 (2014).
36. C. S. Hughes, L. M. Postovit, G. A. Lajoie, Matrigel: a complex protein mixture required for optimal growth of cell culture. *Proteomics*. **10**, 1886–1890 (2010).
37. M. Schoumacher, A. Glentis, V. V. Gurchenkov, D. M. Vignjevic, Basement membrane invasion assays: Native basement membrane and chemoinvasion assay. *Methods Mol. Biol.* **1046**, 133–144 (2013).
38. M. Saghizadeh *et al.*, A simple alkaline method for decellularizing human amniotic membrane for cell culture. *PLoS One*. **8** (2013), doi:10.1371/journal.pone.0079632.
39. O. De Wever *et al.*, Modeling and quantification of cancer cell invasion through collagen type I matrices. *Int. J. Dev. Biol.* **54**, 887–896 (2010).
40. C. H. Teh, R. T. Chin, On the Detection of Dominant Points on Digital Curve. *Pami*. **11**, 859–872 (1989).
41. C. B. Barber, D. P. Dobkin, H. Huhdanpaa, The quickhull algorithm for convex hulls. *ACM Trans. Math. Softw.* **22**, 469–483 (1996).
42. N. Otsu, A Threshold Selection Method from Gray-Level Histograms. *IEEE Trans. Syst. Man Cybern.* **9**, 62–66 (1979).
43. K. Hotary, X. Y. Li, E. Allen, S. L. Stevens, S. J. Weiss, A cancer cell metalloprotease triad regulates the basement membrane transmigration program. *Genes Dev.* **20**, 2673–2686 (2006).
44. D. Q. Matus *et al.*, Invasive Cell Fate Requires G1 Cell-Cycle Arrest and Histone Deacetylase-Mediated Changes in Gene Expression. *Dev. Cell*. **35**, 162–174 (2015).
45. W. Halfter *et al.*, The Bi-Functional Organization of Human Basement Membranes. *PLoS One*. **8**, 1–14 (2013).
46. S. Taniguchi, T. Iwamura, T. Katsuki, Correlation between spontaneous metastatic potential and type I collagenolytic activity in a human pancreatic cancer cell line (SUIT-2) and sublines. *Clin. Exp. Metastasis*. **10**, 259–266 (1992).
47. A. Gandalovičová *et al.*, Migrastatics—Anti-metastatic and Anti-invasion Drugs: Promises and Challenges. *Trends in Cancer*. **3**, 391–406 (2017).
48. A. Rice, L. Julian, M. Olson, A. del Río Hernández, Traction force microscopy with elastic pillars for quantification of forces during cell apoptosis. *Converg. Sci. Phys. Oncol.* **2**, 44501 (2016).
49. A. J. Rice *et al.*, Matrix stiffness induces epithelial-mesenchymal transition and promotes chemoresistance in pancreatic cancer cells. *Oncogenesis*. **6**, 1–9 (2017).
50. A. V. Nguyen *et al.*, Stiffness of pancreatic cancer cells is associated with increased invasive potential. *Integr. Biol.* **8**, 1232–1245 (2016).
51. L. O'Clair *et al.*, Quantification of Cell Migration and

Invasion Using the IncuCyte™ Chemotaxis Assay. *Ess. Biosci.* (2015).
52. L. R. Cisneros Castillo, A. D. Oancea, C. Stüllein, A. Régnier-Vigouroux, A Novel Computer-Assisted Approach to evaluate Multicellular Tumor Spheroid Invasion Assay. *Sci. Rep.* **6**, 1–16 (2016).
53. S. Doyle, M. Brandwein-Gensler, J. Tomaszewski, Quantification of tumor morphology via 3D histology: application to oral cavity cancers. **979112**, 979112 (2016).

Abbreviations

BM, Basement membrane; ECM, Extra-cellular matrix; EMT, Epithelial-to-mesenchymal transition; BME, Basement membrane extract; PBS, Phosphate buffered saline; PCR, Polymerase chain reaction; PDAC, Pancreatic Ductal Adenocarcinoma; PFA, Paraformaldehyde; BSA, Bovine Serum Albumin; 3D, Three-Dimensional; ROI, Region of interest

Supplementary Material

Supplementary Figure 1: Design for mesentery extraction scaffolds made using Rhino 5. Each cylinder has an external diameter of 0.7 cm

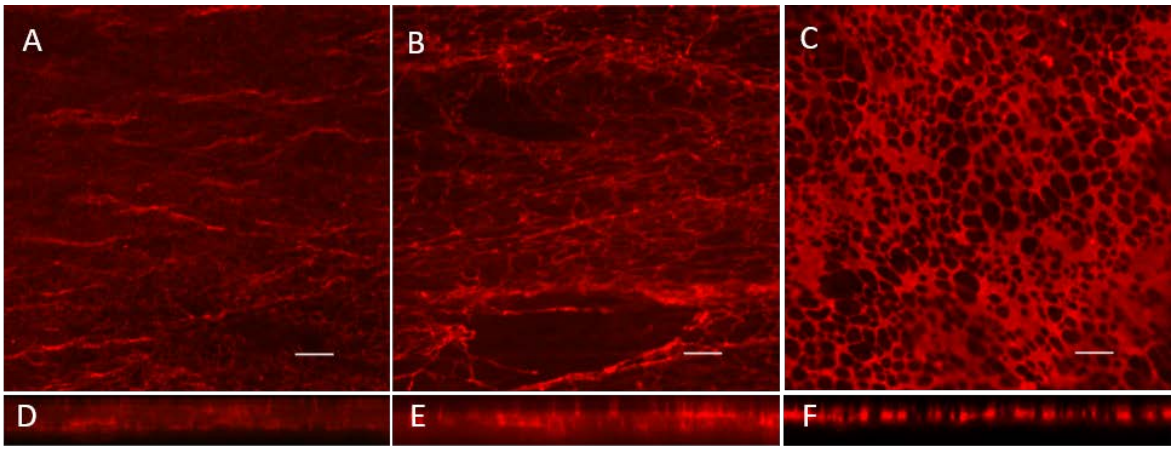

Supplementary Figure 2. Optimisation of immunostaining. (A-C) Collagen IV primary antibody was used to optimise the staining protocol. (A) Protocol from Schoumacher *et al.* 2013 was used (PEM was replaced with PBS). (B) Increasing permeabilisation and initial wash step durations leads to more uniform and higher intensity staining. (C) Adding the blocking treatment before primary antibody treatment reduces nonspecific binding. (D-F) z-Stacks for A-C respectively shows increase in staining specificity. Scalebars are 10 µm.

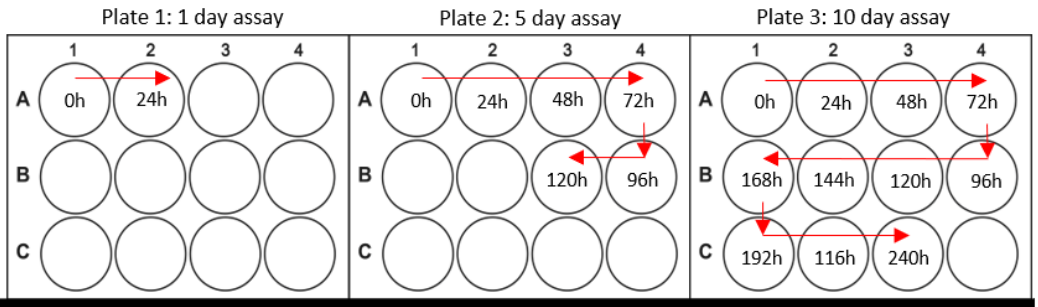

Time (h)	Plate 1	Plate 2	Plate 3
0	i. Mesentery placed on complete media ii. Cells seeded onto mesentery in serum-free media	i. Mesentery placed on complete media ii. Cells seeded onto mesentery in serum-free media	i. Mesentery placed on complete media ii. Cells seeded onto mesentery in serum-free media
24	i. Mesentery fixed.	i. Mesentery moved to complete media in well A2	i. Mesentery moved to complete media in well A2
48		i. Mesentery moved to complete media in well A3 ii. <u>Bottom of well A2 imaged</u>	i. Mesentery moved to complete media in well A3 ii. <u>Bottom of well A2 imaged</u>
		⋮	⋮
120		i. Mesentery fixed ii. <u>Bottom of well B4 imaged</u>	i. Mesentery moved to complete media in B3 ii. <u>Bottom of well B4 imaged</u>
			⋮
240			i. Mesentery fixed ii. <u>Bottom of well C2 imaged</u>

Supplementary Figure 3. Detailed step-by-step procedure for daily handling, imaging and fixation of mesenteries and wells as required for day 1 to 10 results. Underlined steps indicate invasion cell count assay.